

Research

Numerical and experimental analysis of 3D printer hot ends

Michael Hutchinson¹ · Andrew O'Donohue¹ · Babak Eslami¹ · Kamran Fouladi¹

Received: 28 November 2023 / Accepted: 10 April 2024

Published online: 16 April 2024

© The Author(s) 2024 [OPEN](#)

Abstract

The design of the hot end plays a critical role in additive manufacturing, especially in material extrusion. Yet the melt flow behavior within the hot end assembly has not been explicitly presented regarding the hot end design. The present study intends to fill this knowledge gap by employing a two-phase approach to investigate the melt dynamics through three commercially available hot ends. The hot ends considered are E3D v6 Standard, v6 Gold, and Revo Six, which were chosen based on brand, design, and functionality. In Phase 1, an experimental apparatus was developed to assess the impact of feeding rate and extrusion temperature on the outlet temperature, outlet velocity, and under-extrusion percentage of extruded polymer. In Phase 2, the polymer flow through each hot end is explored utilizing a computational fluid dynamics model, which was validated using data obtained in Phase 1. It was determined that the filament feeding rate is the most influential parameter in polymer extrusion and that Revo Six's symmetrical design affects the stability of extrusion. It was also revealed that the thermal evolution of the melted filament within the hot end assembly is directly affected by the length of the heating region and the polymer's material properties. The experimental and numerical procedures developed in this investigation can be useful to 3D printing users and manufacturers in selecting a hot end assembly based on application requirements.

Article Highlights

- The role of hot ends on 3-D printing performance were investigated using three commercially available hot ends through a combined numerical and experimental investigation.
- Hot end's heating length and polymer's properties will determine thermal evolution of the melted filament within the hot end assembly
- The feed rate strongly impacts the melt front location in hot ends.

Keywords Hot ends · Material extrusion · Polymer · 3D printing · Computational fluid dynamics

1 Introduction

Material Extrusion (MEX) technique has garnered significant attention in additive manufacturing due to its ease of use, low cost, and ability to quickly modify the fabrication of complex parts [1]. The quality of MEX printed parts is often assessed using metrics such as surface finish smoothness, geometrical accuracy, and effective material properties. However, the quality of a part may depend on parameters such as filament material properties, feeding rate,

✉ Babak Eslami, beslami@widener.edu | ¹Department of Mechanical Engineering, Widener University, Chester, PA 19013, USA.



extrusion temperature, and environmental conditions [2]. For example, the temperature and humidity of the printing environment have been shown to play significant roles in print quality [3].

The hot end assembly (HEA) is a critical component in MEX 3D printers, playing a vital role in the printing process. This component is essential for efficient, high-quality MEX printing for a given application. For example, the HEA is responsible for melting the polymer by maintaining a setpoint temperature as the melted polymer filament is extruded onto a heated surface [3]. The melting process occurs in the HEA's liquefier and nozzle region, and a properly maintained temperature in this region ensures the continuous extrusion of material. In contrast, the heat sink region in the HEA must ensure polymer remains solid before entering the liquefier to prevent jams [4]. Finally, a lower pressure drop in the nozzle reduces the likelihood of buckling of the feedstock [5].

Due to the difficulty and complex nature of observing the polymer melt flow within the hot end cavity, numerical modeling has been employed to capture flow phenomena. Pigeonneau et al. developed a CFD model to analyze the temperature evolution of the filament during the flow through the hot end. They used the measurements obtained by Peng et al. to validate their simulations and concluded that variable thermal contact would prohibit the polymer from reaching the temperatures measured by Peng et al. This conclusion is a direct contradiction to the work performed by Phan et al., who determined that the polymer will never reach the temperature specified by the heated liquefier. Phan et al. suggested that fouling and/or surface irregularities will cause this drop in temperature. Xu et al. furthered this work by exploring the relationship between polymer flow and viscoelastic stresses, demonstrating that the influence of the viscoelastic properties during extrusion is more significant than the viscous effect, particularly at faster extrusion speeds [6]. Pricci et al. extended the above work by incorporating the Cross-WLF rheological model while Mishra et al. implemented both the improved Cross-WLF viscosity model as well as the variable PVT density model in their study [7]. The distribution of extrusion parameters such as pressure, temperature, and viscosity inside the liquefier were compared to predict the steady-state extrusion profile at the outlet of the nozzle. This profile was then transferred to a strand deposition model to compare the variable viscosity and density model against the constant property's models. Mishra et al. concluded that the introduction of the Cross-WLF, PVT, and velocity profile showed strong correlations to the experimentally determined thermal swelling and contraction that occurs after deposition by Duty et al. [8].

The experimental assessments of hotend assemblies by manufacturers and companies are typically proprietary and not shared in published literature. However, the currently practiced HEA calibrations involve a process of printing a part with various changes in process parameters until a desired result is achieved [9]. Typical parameters analyzed in calibrations include the extrusion temperature, feed rate, nozzle diameter, filament diameter, and fan cooling performance. It should be noted that these variables do not consider additional constraints on the system, such as the 3D printer build quality or the performance of the hardware and software that controls the printing process (such as sensors or motors). Moreover, there is a lack of systemic and in-depth research on the performance of the HEA for printing polymer-based components under specified printing conditions such as temperature, feed rate, relative humidity, etc.

1.1 Motivation and objectives

The popularity of MEX and the significant role of HEA in the printing process requires a systemic and in-depth investigation of the performance of this vital component. The current effort aims to shed light on the melt flow dynamics of the hot end and its effects on the material extrusion printing process. More specifically, the present investigation aims to establish correlations between hot end design and printing stability while accounting for large variations in printing setups and hardware.

The goal of this study is pursued by employing a combined numerical and experimental investigation of three commercially available hot ends chosen based on brand, design, and functionality. The investigated hot HEAs are E3D (1) v6 Standard, (2) v6 Gold, and (3) Revo Six. It should be noted that the v6 Standard serves as the baseline for analysis as it has been the pioneer among the current selection of hot ends. Moreover, the v6 Gold is a modified version of the v6 Standard with improved thermal stability and manufacturing precision, and the Revo Six has a significantly distinctive design comparatively due to its cylindrical heating element and interchangeable nozzles. The combination of all three will serve as the outline for evaluating and investigating the hot end assemblies.

The successful completion of this study should produce a procedure for systemic and comprehensive benchmarking of the performance of current and future commercially available and future hot-end assemblies. Therefore, the results from

Fig. 1 Testing apparatus used for experimental extrusion studies

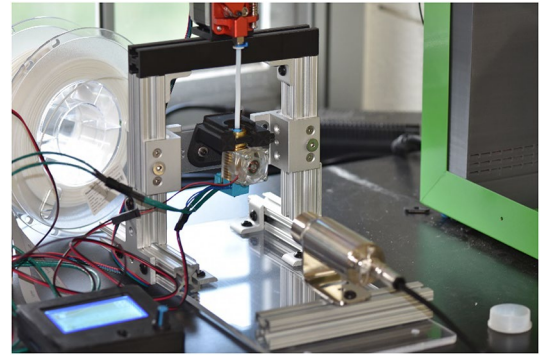
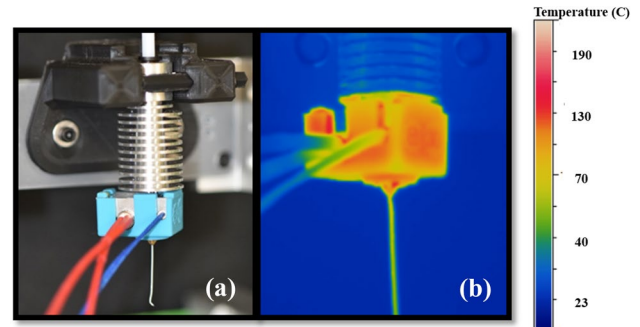


Fig. 2 **a** v6 Standard hot end during extrusion, **b** thermal image of the hot end during testing



this work can directly help 3D printer manufacturers enhance their printers' capabilities, optimize their printer design, and enhance their printing guidelines for a given application. In the manuscript, the experimental setup in addition to the theory for setting up the simulation model are discussed. Afterwards, the results and the corresponding analysis is provided. Finally, the conclusions and future work are listed.

2 Materials and methods

2.1 Experimental setup

A testing apparatus, shown in Fig. 1, was designed and employed in this study to simulate the functionality of a typical 3D printer with modular hot end assembly for easy access and change. This apparatus aimed to control the variability of parameters of interest while reducing the total number of variables associated with typical desktop 3D printers. The apparatus consisted of a direct drive (2 gear) extruder with a Bowden tube attached to limit buckling of the feed stock. Integration between the printer firmware, *Marlin* [10, 11], and the hardware components of each hot end (thermistor, heating cartridge, and fans) was performed via the GUI host *Pronterface* [11].

Infrared (IR) thermal imaging was used to directly observe the filament extruded from the HEA. The *Optris XI* thermal camera was utilized to measure the filament temperature around the surface. The maximum error of the thermal camera was taken as the manufacturer's specific uncertainty of ± 2 °C [12]. The thermal camera's emissivity and transmissivity parameters were verified using a thermocouple and digital multimeter by measuring an object of known temperature and comparing this value to the thermal camera's output. The extrusion temperature measurements also consisted of setting the hot end to the desired extrusion temperature and setting the desired feed rate and filament length through G-code commands. For each hot end, the temperature was set to 190, 215, and 240 °C, while the feed rate varied from 0.83 to 3.33 mm/s for each extrusion temperature, corresponding to typical MEX printing nominal feed rates of 50 to 200 mm/min. An example of a thermal image taken during extrusion is shown in Fig. 2.

The apparatus was equipped with a Nikon D750 camera for measuring the velocity of the filament exiting the HEA. The camera was configured to record with a frame rate of 60 fps to obtain the centerline velocity at the nozzle exit. The image processing was performed via *ImageJ* by selecting a datum location, specification of the frame rate, and then calculating the change in position of the filament over the entire extrusion.

It was also important to consider the auxiliary effects of feed rate and extrusion temperature on the likelihood of material under-extrusion, caused by the material properties of melted polymers. The under-extrusion percentage (%*UE*) is defined by Eq. 1, similar to the study performed by Hermann [9],

$$\%UE = \left(\frac{W_{actual}}{W_{expected}} - 1 \right) \times 100 \quad (1)$$

where W_{actual} is the measured mass of filament after extrusion. The parameter $W_{expected}$ is the expected filament mass determined by

$$W_{expected} = Q_f \rho_f \Delta t \quad (2)$$

where Q_f is the material's volumetric flow rate, and ρ_f is the filament density assumed to be 0.00124 g/mm³ [13]. The parameter Q_f is determined by Eq. 3 where f_o (mm/s) is the feed rate, L_f (mm) is the length of requested filament, and d_f (mm) is the filament diameter set as 0.4 mm.

$$Q_f = f_o L_f d_f \quad (3)$$

2.2 Numerical setup

Computational fluid dynamics (CFD) modeling, based on ANSYS® FLUENT 2020 R1 [14], was employed to simulate the polymer flow inside each hot end assembly with a concerted effort to model each HEA as geometrically accurate as possible. The CFD models included transient conjugate heat transfer simulation in determining the outlet temperature, outlet velocity, and the dynamic viscosity of the extruded polymer for comparison of various hot ends. These parameters were used to describe essential characteristics of the flow, such as the effects of pressure, viscosity, liquefier length, and the fully melted region. Moreover, the transition from solid to liquid–solid to fully liquid is achieved via the Solidification and Melting Model in FLUENT.

Figure 3 presents the typical geometry and surface mesh of the polymer flow hot end model, where geometrical dimensions were obtained from E3D's website [15]. The fluid domain for each model was captured via volume extraction in the solid modeler and then coupled with the solid domain via conjugate heat transfer. A structured mesh (Fig. 3b), using the Multi-Zone Quad/Tri Method, was utilized to maximize the accuracy of the numerical results. Furthermore, mesh layer inflation was employed to ensure that the higher temperature gradients between the barrel wall and filament domains were captured.

Fig. 3 a Solid model geometry, b surface mesh of the Revo Six polymer flow model

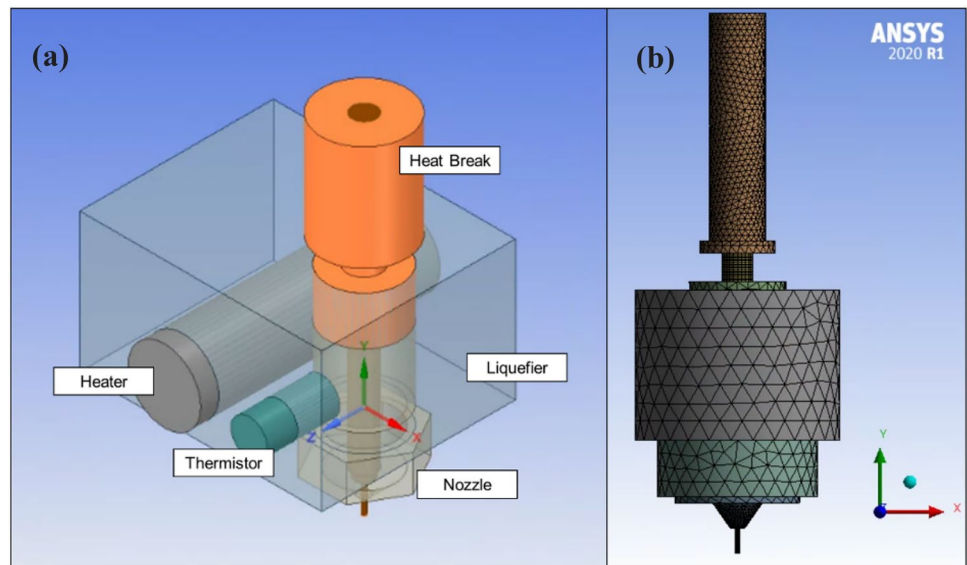


Fig. 4 Nodal temperatures along the filament diameter for various mesh qualities

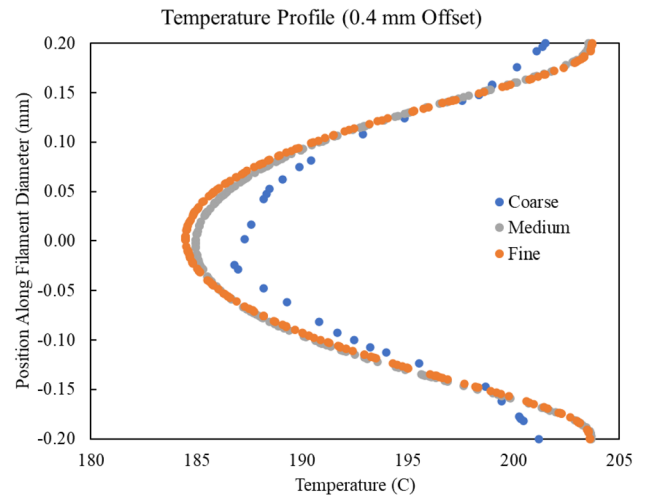


Table 1 Properties of PLA used for the numerical simulations [17]

Thermal properties		Rheological properties	
ρ	1122.80 kg/m ³	τ^*	129,000 Pa
C_p	2140 J/kg K	n	0.3846
k	0.180 W/m K	D_1	2.05×10^7 Pa s
		A_1	16.71
		T^*	373.15 K
		A_2	51.60 K

A grid refinement study was performed to obtain a mesh-independent solution using three meshes of varying refinement and the melt (temperature) profiles near the outlet as the objective variable. The three mesh with a total mesh count of 3×10^6 elements (Coarse), 5×10^6 elements (Medium) and 7×10^6 elements (Fine) were generated using similar mesh settings. Figure 4 presents the grid independence study results, indicating a consistent temperature profile for Medium and Fine meshes. Based on the grid independence study, the Medium mesh was chosen for further investigation due to its lower run time and no significant degree of error.

The inlet boundary condition in these simulations was inlet velocity, corresponding to the requested feeding rates, with specified temperature. The inlet temperature was set at slightly above the Polylactic acid (PLA) glass transition temperature of 60 °C ensuring polymer melt enters the domain as fluid and above its glass transition temperature [16]. The outlet pressure set at ambient pressure was used for the outlet boundary condition for all cases. Walls were treated with a zero-slip condition based on a similar assumption by Mishra et al. that the polymer enters the domain in a fully liquid state [17]. Furthermore, variable thermal contact between the filament surface and various HEA walls (heating cartridge and hot end liquefier) was employed to increase accuracy based on previous studies [18]. The temperature of the heating cartridge for each hot end was governed by a volumetric heat flux energy source term, which was validated using the temperature vs. time curves of each hot end assembly when set to a specific extrusion temperature.

For the Solidification and Melting Model, the density of the PLA was assumed constant when at the solidus temperature, whereas the density was varied with the PVT model at the liquidus temperature. The solidus and liquidus temperatures for PLA were assumed at 140 °C (413 K) and 155 °C (428 K), respectively [1]. Finally, the latent heat of fusion L was assumed to be 0.001 J/kg to predict the liquid-fraction evolution during the melting. Finally, fluid viscosity was modeled using the Cross-WLF viscosity model. A user-defined function was implemented into the solver to compute cell temperature and the shear rate at each time step. Material property assumptions and fitting parameters for PLA are summarized in Table 1.

Fig. 5 Temperature versus time plot for 0.83 mm/s (50 mm/min) and 190 °C

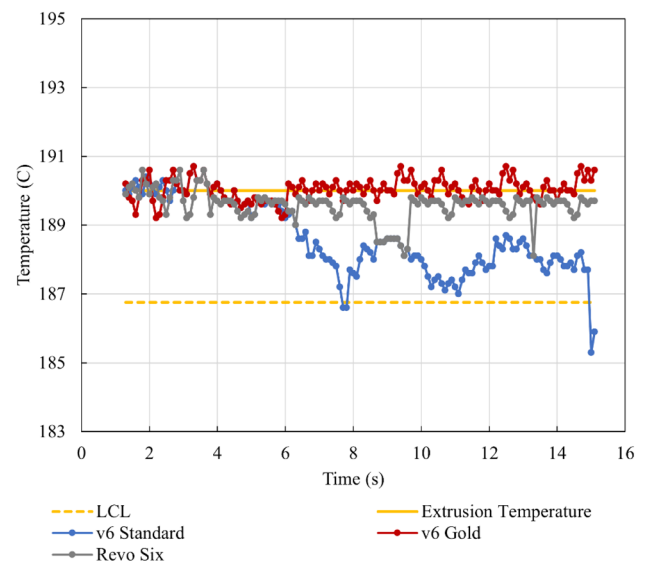
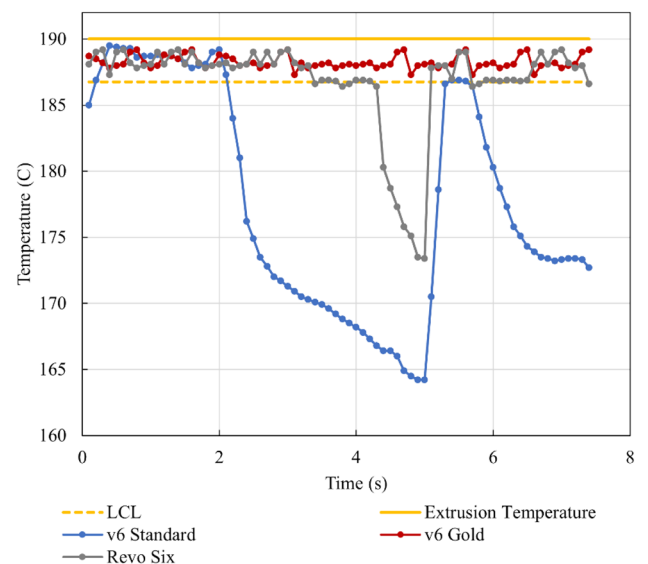


Fig. 6 Temperature versus time plot for 3.33 mm/s (200 mm/min) and 190 °C



3 Results

3.1 Experimental results

Figure 5 presents the temperature of the extruded polymer over time for all three hot ends with the specified extrusion temperature set at 190 °C at a feed rate of 0.83 mm/s (50 mm/min), simulating a slow printing scenario. The lower control limit (LCL) is plotted as the dotted line in Fig. 5. LCL is defined as the temperature point where observable slippage of the extruder pinch-rollers was observed, causing under-extrusion of the filament. It is important to note that the fluctuations from the setpoint temperature may be a result of PID control and thermal imaging accuracy and measurement variation.

While some temperature variation was observed at the 0.83 mm/s (50 mm/min) feed rate, this variation was significantly higher at the high flow rate speed scenario of 3.33 mm/s (200 mm/min), as demonstrated in Fig. 6. Figures 5 and 6, considered together, indicate that the relatively stable temperature profile of the v6 Gold resulted in stable extrusions. Conversely, the temperature fluctuations during the extrusions with the v6 Standard and Revo Six caused significant under-extrusion of material. Importantly, the v6 Standard experienced two under-extrusion events, whereas the Revo Six experienced one. The under-extrusions occurring at the higher feed rates may have caused

Fig. 7 Outlet velocity versus feed rate for the v6 Standard hot end

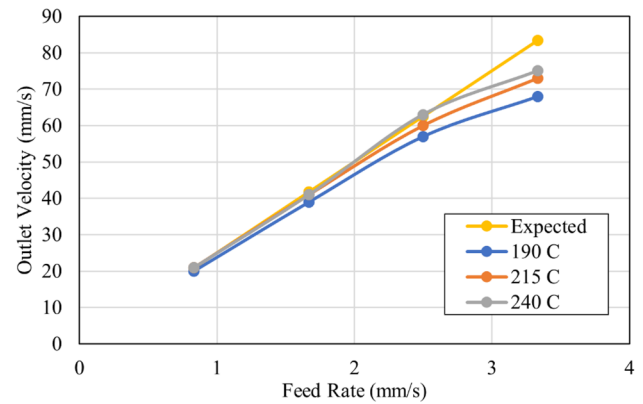
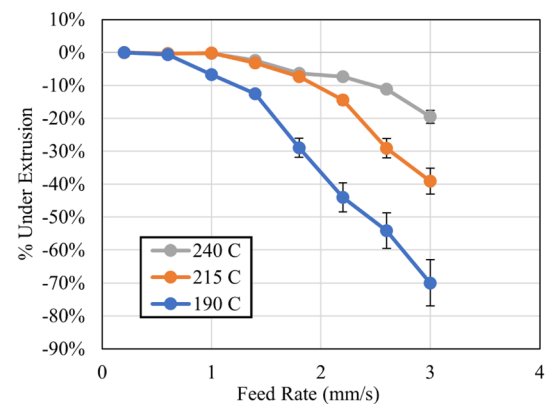


Fig. 8 Under-extrusion % for the v6 Standard for various extrusion temperatures



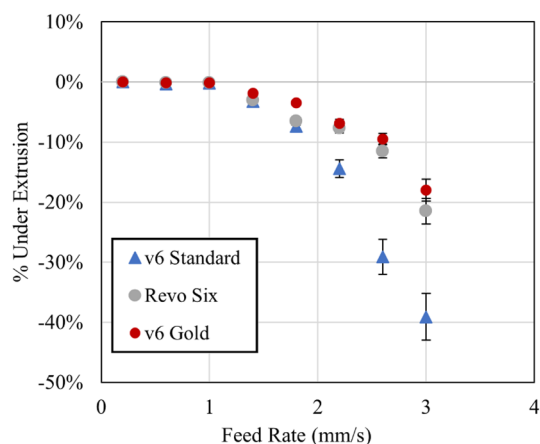
the under-melting of the polymer resulting in increased viscosity. This increase in viscosity can directly increase the pressure in the hot end barrel, causing the extruder pinch-rollers to slip.

It is evident in Fig. 7 that the measured outlet velocity increases with higher extrusion temperatures, which may be due to the polymer becoming less viscous at higher temperatures. However, and more importantly, Fig. 7 results indicate that temperature variation has a higher impact on deposition velocity as the feed rate increases. At the lowest feed rate, the measured outlet velocity is comparable to the expected velocity. However, the measured outlet velocity is lower than the expected value at higher feed rates, and this difference is greater at lower set temperatures. Therefore, it can be argued that the deposition velocity could vary due to thermal fluctuations as the printer nozzle moves along the printing substrate. This finding is important as velocity variation has been shown to result in non-uniform melt deposition [17].

The impact of the extrusion temperature on the amount of polymer extruded was investigated on the v6 Standard by varying the set temperature as the filament feed rate changed. In this measurement, the feed rate ranged from 0.2 to 3 mm/s with the extrusion temperature set at 190 °C, 215 °C, and 240 °C. As presented in Fig. 8, the extrusion temperature is shown to directly affect the amount of under-extruded material. Furthermore, the amount of under-extrusion is larger at higher feed rates due to the feeding force causing more extruder slippage. It should be noted that each data point shown in Fig. 8 is an average weight of three filament samples and that the error bars account for a measurement error of 2%.

The role of hot end design on under-extrusion percentage was investigated at the nominal extrusion temperature of 215 °C. The result of this investigation is presented in Fig. 9, indicating that the amount of under-extrusion for all three hot ends remains similar up to 1.8 mm/s (108 mm/min). However, the hot ends performed differently at higher feed rates. The v6 Gold performed the best with the least under-extrusion, while the v6 Standard under-extruded by nearly 40% at the highest feed rate.

Fig. 9 Under-extrusion % for various hot ends at 215 °C



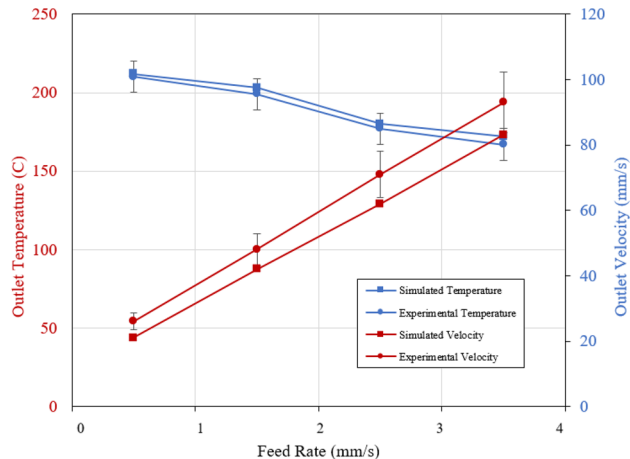
3.2 Numerical results

The computational efforts undertaken in this study were developed to help understand the underlying reasons for the performance of hot ends, which were obtained in the experimental phase of the investigation. The melt evolution inside each hot end was the primary focus of these CFD models. The baseline polymer flow CFD model was validated using experimentally acquired average exit temperature (on the filament surface) and average outlet velocity. Results presented in Fig. 10 indicate both the measured outlet velocity and temperature followed trends similar to the simulation. Error bars represent a percentage measurement deviation associated with both the thermal imaging camera and the NIKON camera. All three hot end models were validated similarly, demonstrating comparable results.

The initial objective of the numerical effort was to determine if the filament exiting the hot ends reached the set extrusion temperatures. Figure 11 shows the temperature difference (ΔT) between the polymer set extrusion temperature (T_{ext}) and the predicted exit temperature (T_{out}) at varying feed rates for various set temperatures. Defined as $\Delta T = T_{ext} - T_{out}$, this temperature differential is only a few degrees at lower feed rates for all hot ends. However, the difference is exacerbated at higher feed rates and reaching to 40 to 60 °C range at 3.5mm/s feed rate. The v6 Standard consistently demonstrated the worst performance compared to the others. Conversely, Revo Six showed slightly better capabilities to produce a higher outlet temperature, which may be attributed to its longer liquefier section and cylindrical shape heating cartridge.

The Revo Six's cylindrical heating block (cartridge) design may be responsible for the more uniform temperature distribution of the melted polymer resulting in the lower temperature differential. The temperature distribution in the heating block of the v6 Standard and Revo Six set for an extrusion temperature of 215 °C and feeding rate of 1.67 mm/s are illustrated in Fig. 12. Figure 13 presents the filament's temperature contours at the nozzle outlet cross-section for the same simulation case. In these plots, Revo Six shows a more axisymmetric temperature distribution

Fig. 10 Validation data for the v6 Standard polymer flow model. Note: All values are nominal (215 °C extrusion temperature, 100 mm/min feed rate). Error bars represent uncertainty associated with the measurement technique performed



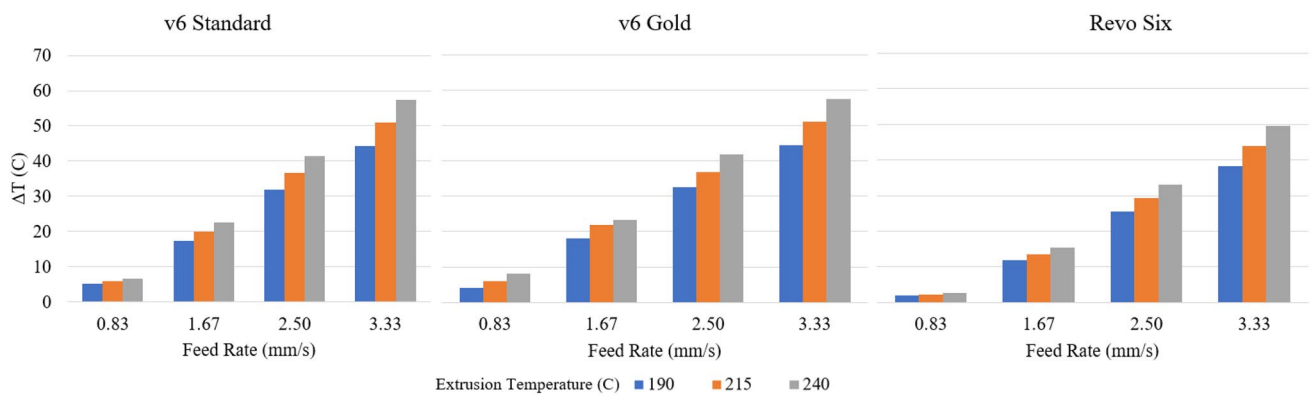


Fig. 11 Difference between the extrusion temperature and the filament outlet temperature with varying feed rate

Fig. 12 Contours of temperature for **a** the v6 standard and **b** Revo six heater blocks

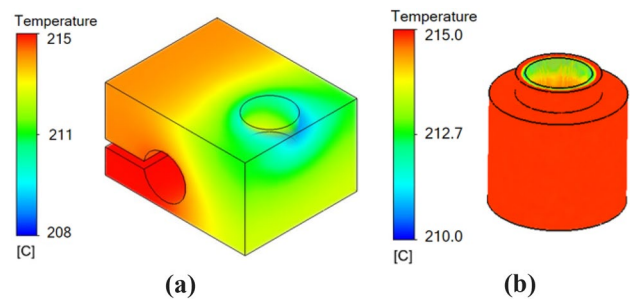
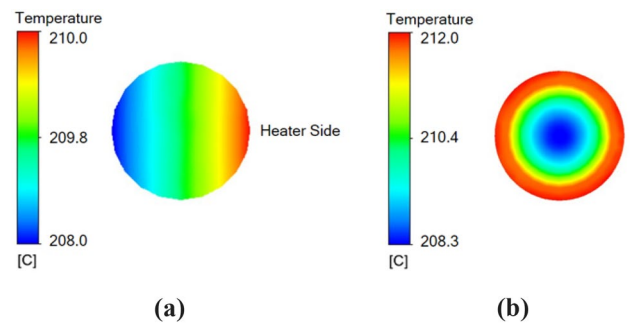


Fig. 13 Contours of temperature for the filament cross-section at the nozzle outlet for **a** v6 standard, **b** Revo six

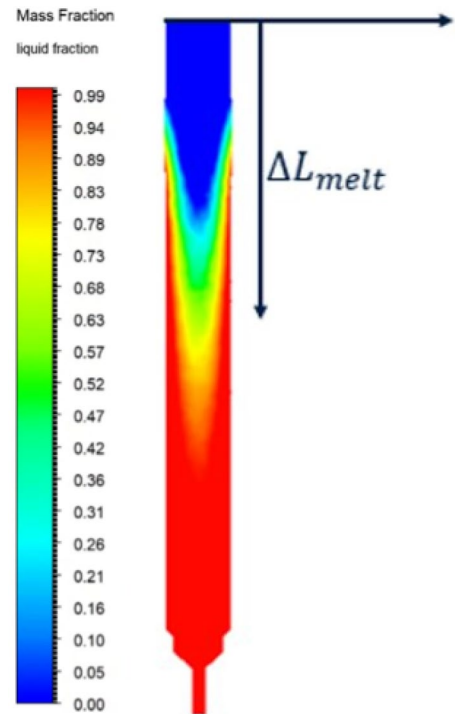


with a more uniform core due to its cylindrical heating block, “HeaterCore.” Specifically, Revo Six’s cylindrical design allowed for more uniform heating and increased temperature at its lowest point (210 °C). Conversely, the significant temperature variation in the heating block of v6 Standard and Gold (not shown) can be attributed to the block’s asymmetrical design, which further emphasizes the heating block’s significant impact on the filament’s melt profile.

The disparity between the extrusion set temperature and the filament’s outlet temperature was further investigated by examining the effects of the feed rate and extrusion temperature on the melt front of the polymer inside the hot end barrel. The melt front is defined here as the axial distance measured from the nozzle’s inlet to the location where the polymer is fully melted beyond the glass transition region (taken as 60 °C) and has reached a liquid fraction of 1.0 (Fig. 14). In polymer extrusion cases, it has been studied that a varying melt front can impact the deposition process that may cause plugged flow in the nozzle, and possible increased likelihood of under-extrusion of material [16].

Similar to the study by Ufodike and Nzebuka [19], the melt front in each simulation case was tracked by observing the solidification and melting front of the fluid using an enthalpy-porosity formulation. In this approach, the liquid–solid “mushy zone” was treated as a porous zone with porosity equal to the liquid fraction of PLA [14]. Furthermore, appropriate momentum sink terms were added to the momentum equations to account for the pressure drop caused by the presence of solid material [14].

Fig. 14 Example of the varying melt front location (ΔL_{melt}) for a nominal extrusion temperature



The melt front for each hot end was studied for a full range of feed rates and extrusion set temperatures and presented in Fig. 15. In this figure, additional extrusion temperatures are provided for v6 Standard for more details but are omitted for other hot ends for clarity. It is evidenced by the results presented in Fig. 15 that feed rate is the dominating process parameter impacting the melt front location in each hot end, as this location varied by nearly 2 mm as the feed rate increased by 0.83 mm/s (50 mm/min). Additionally, the v6 Standard's melt front location decreased by nearly 1 mm with every 10°C increase in the extrusion temperature. However, the results indicate that the v6 Gold and Revo Six were able to heat up the filament to fully melt condition at shorter liquefier distances compared to the v6 Standard. The difference in melt front locations for v6 Standard and Revo Six is approximately 3 mm for PLA nominal printing conditions of 215°C temperature and 1.67 mm/s (100 mm/min) feed rate.

Previous studies have suggested that non-uniform nozzle outlet velocity and thermal profiles with steeper slopes adversely affect filament deposition [17, 18]. Therefore, these profiles for each hot end were examined at the PLA nominal printing conditions, with a summary of results presented in Fig. 16. Comparable to the previous studies [8, 17–19], the results of the present study indicated parabolic profiles for the temperature and velocity at the nozzle exit with minimum temperature and maximum velocity at the centerline. Moreover, the temperature gradient for the v6 Standard is shown to be larger and asymmetrical compared to the Revo Six, consistent with previously discussed results. On the other hand,

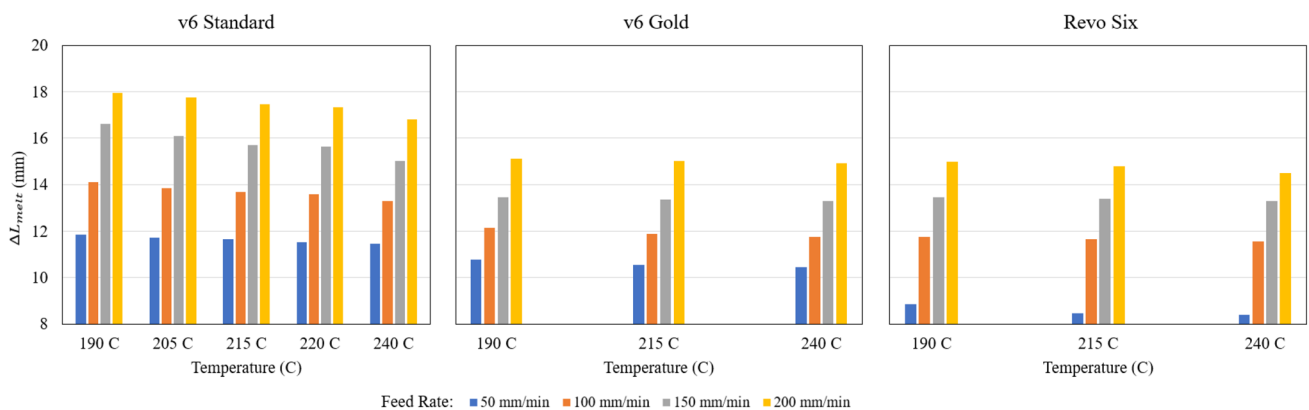


Fig. 15 Melt front locations for various feed rates and extrusion temperatures

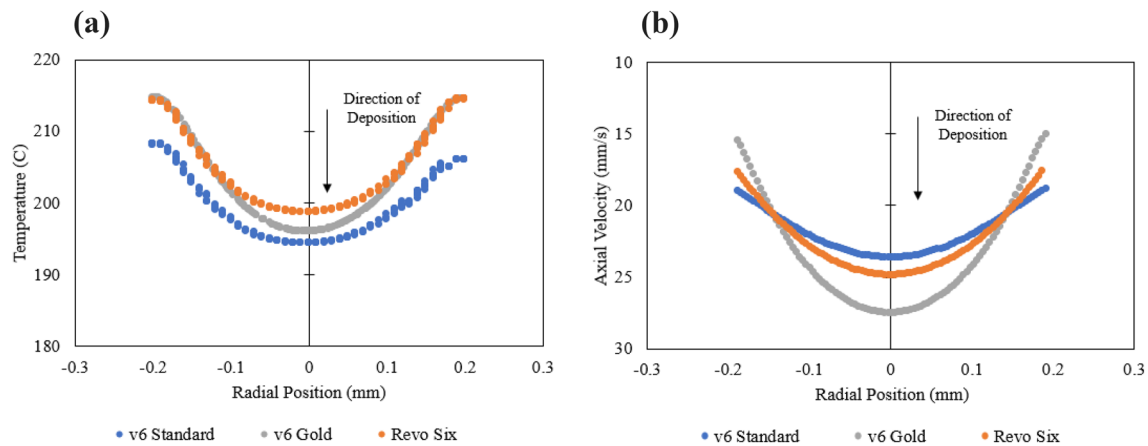


Fig. 16 **a** Temperature and **b** velocity profiles for nominal printing conditions

CFD results predicted (not shown here) that the v6 Gold exhibited a noticeably higher peak axial velocity that is 3.5 mm/s and 6 mm/s faster than the Revo Six and v6 Standard, respectively.

Because of the temperature dependency on the viscosity of PLA, the temperature differences between each liquefier design affect the melt dynamics of the polymer. Specifically, given that the Revo Six heated the polymer more efficiently, the polymer viscosity at the outlet, η , was found to be approximately 300 Pa s. In contrast, the outlet viscosity for the v6 Standard was nearly 350 Pa s, a difference of 15.3%. The velocity profiles in Fig. 16b indicate that this variation in the polymer viscosity between each HEA affected the exit velocity profiles considerably. Given the profiles presented in Fig. 16b, it is important to comment on the relation between printhead speed and extrusion speed. This relation can be characterized by the velocity ratio, V_{out}/V_{print} , where V_{out} is the peak axial velocity of the polymer and V_{print} is the translational speed of the printhead. Previous analysis performed by Gosset et al. has shown that the strand morphology is greatly affected for velocity ratios less than 1.0 ($V_{out} < V_{print}$) [20]. That is, less polymer is being extruded than the printed model required. Conversely, for velocity ratios greater than 1.0 ($V_{out} \geq V_{print}$), over-extrusion of extruded polymer is likely.

Based on the above-mentioned study, and an enhanced understanding of the melt dynamics of various hot end models, we have investigated the effect of layer height based on a given feed rate, extrusion temperature, and hot end model on dimensional inconsistencies in the deposited strands. While previous efforts have endeavored to improve upon the accuracy of polymer deposition modeling, they all omit an accurate solid model for the hot end assembly [8, 21–24]. While Serdeczny et al. developed a generalized model to predict the variation in single-strand cross-sectional shapes for various velocity ratios and layer heights, the model was assumed to be isothermal, with constant density and constant viscosity [18]. Mishra et al. proved that the introduction of both a pressure–volume–temperature variable density model, and the Cross-WLF viscosity model improved the accuracy of the predicted cross-sectional areas of the deposited strands [17]. However, the model incorporated by Hutchinson [25], which is used in this study, employs both the work performed by Serdeczny et al. as well as the improved model by Mishra et al. to predict the varying strand cross-sections. In order to apply the temperature and velocity profiles in a practical manner, the hot end flow model was extended to include the deposition of melted filament onto a heated printing substrate. Hutchinson's model [25] explores the implementation of this Volume-of-Fluid (VOF) multiphase model by applying the temperature and velocity profiles as inlet boundary conditions predicted in the hot end flow model. Figure 17 illustrates the boundary conditions and strand deposition predicted by the multiphase model. While symmetry was assumed by Serdeczny, M. P. [18], it was not imposed in this model to capture the asymmetry in the deposited strands' transverse areas. Finally, a mesh refinement study was performed to obtain grid-independent solutions by assessing the convergence of the calculated cross-sectional areas for each deposited strand.

Each cross-section plotted in Fig. 18 was simulated at nominal printing conditions of 215 °C and 100 mm/min for extrusion temperature and feed rate, respectively. All other parameters remained the same for each hot end.

It is apparent that the printed strands exhibit varying dimensional inconsistencies, which can be attributed to the unique velocity and temperature profiles of each hot end established in Fig. 16a, b. Consequently, the predicted variation in the transverse areas of the deposited strands can be used to improve the optimization of slicing software to predict inaccuracies with 3D printing slicers. Specifically, real-time nozzle positional compensation for material distortion caused by both the cooling of the material, as well as the heat transfer between adjacent strands. Moreover,

Fig. 17 Strand deposition model developed by Serdeczny, M. P. [18] and explored by Hutchinson [25] where V_s is the printhead speed, and L_H is the layer height

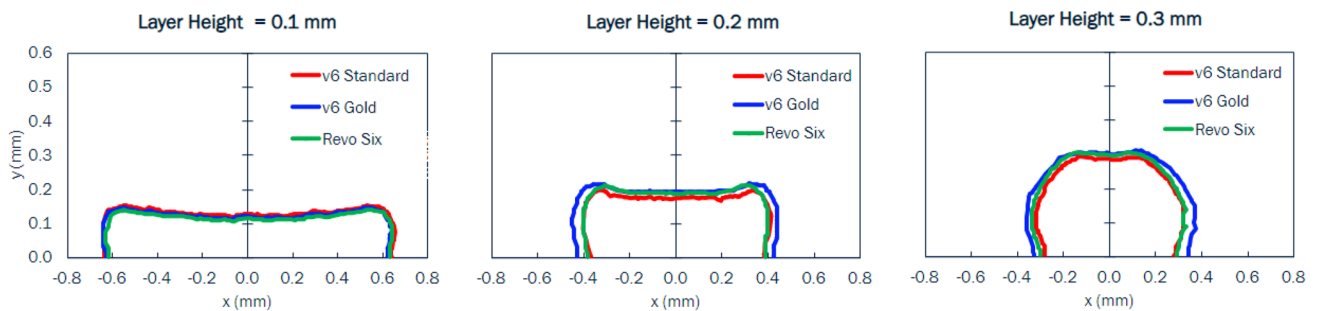
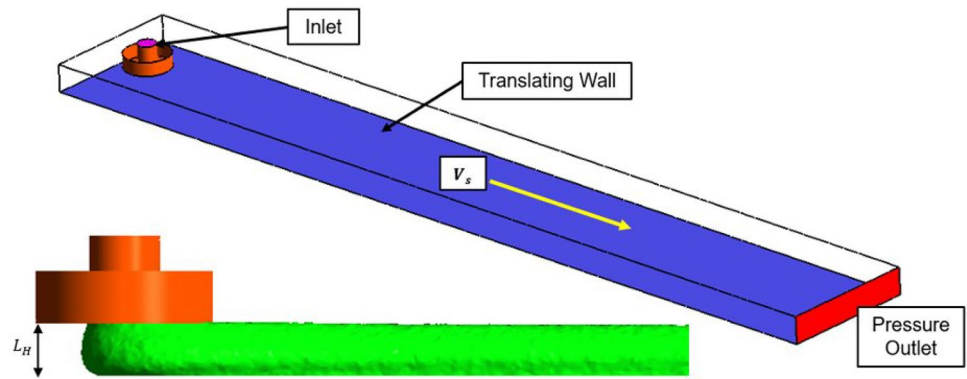
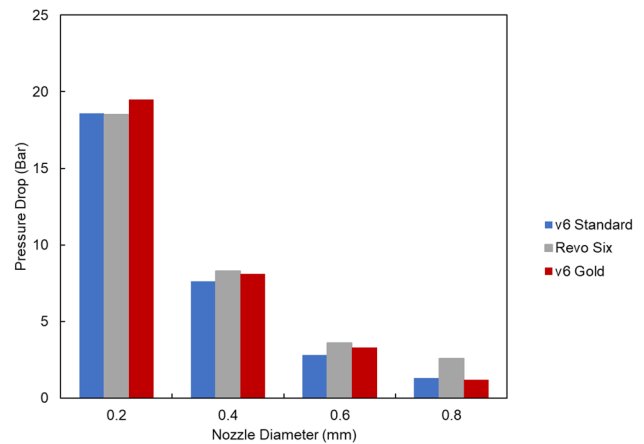


Fig. 18 Transverse strand areas 2 mm from the nozzle outlet for a feed rate of 100 mm/min and an extrusion temperature of 215 °C

Fig. 19 Pressure drop versus nozzle diameter for various hot ends for feed rate of 1.67 mm/s (100 mm/min) and extrusion temperature of 215 °C



adjustment of the filament deposition to aid in overlapping or spacing issues—including adaptive layer height and overhang distances based on the transverse area of the strands.

In various 3D printing applications, it may be necessary to utilize finer strand widths to garner higher degrees of accuracy for a specific print. As a result, by combining smaller strand layer heights and reducing the nozzle diameter, the porosity and bond line densities for various 3D printed cross sections will improve dramatically [18]. In reference to Fig. 19, as the nozzle diameter changes, the pressure drop from the inlet to the outlet of the liquefier region varies tremendously. It is also important to note from the figure that there is minimal variation in the pressure drop between hot end designs, implying that the overall filament temperature is dominated by the outlet diameter with respect to its effect on the pressure drop. In generality, this result can be employed to further describe a hypothetical maximum feed rate, as a higher pressure will cause slipping or buckling of the filament in the extruder. This higher pressure will also result in a deviation in the filament temperature, as the slippage will reduce the flow of material through the nozzle, causing uneven heating.

It should also be mentioned that although this work was focused on one polymer, there are studies done that has looked into the effective material properties of 3D printed parts for different polymers such as ABS, PLA, or PETG [26]. In this study, authors have studied the effect of temperature on FDM 3D printing polymers which can broaden the knowledge in the field. Additionally, it should be noted that energy consumption in the FDM 3D printing is a concern. There are various efforts in the field on the same line to optimize those as well. These are more important now that our work is suggesting different temperatures for hotends. Based on the work done by Harding O. J. et al., it is shown that heated bed insulation did not provide exceptional power consumption saving [27]. The hotend insulation was more distinct, and enclosure insulation findings show there will be increased savings with build times above two hours. Additionally, it was found that modifying print parameters with the goal of saving energy can help the power consumption but the physical modification of the hotend design has not been a successful approach in the field [27].

4 Conclusions

The present study used combined experimental and numerical investigations to focus on the melt flow dynamics through MEX 3D printers' hot ends. Three commercially available and widely used hot ends were considered to understand the role of hot ends on printing performance. Through robust experiments, it was shown that the temperature fluctuations during the extrusions caused more under-extrusion of material for the v6 Standard and Revo Six, whereas the v6 Gold produced more favorable results. At higher feed rates, these temperature variations impacted the deposition velocity, causing non-uniform melt deposition and notable under extrusion. Using v6 Standard as the baseline, it was found that the extrusion temperature directly affected the amount of under-extruded material, with larger under-extrusion at higher feed rates, due to more extruder slippage. In this study, the v6 Gold performed the best among the three hot ends with the least under-extrusion, while the v6 Standard under-extruded by nearly 40% at the highest feed rate. Therefore, the theoretical and experimental findings of this study can be directly used for 3D printing end-users: (1) the key factor in defining the under-extrusion in a hot end is the extrusion temperature, (2) there is a higher chance of under-extrusion at higher feed rates, and (3) v6 Gold or similar hot end models will have minimum under-extrusion.

The extrusion temperature and velocity were further investigated through CFD modeling. The difference between set extrusion and predicted outlet temperatures was significant for all three hot ends at higher feed rates, reaching 40 to 60 °C at 3.5mm/s feed rate. While v6 Standard consistently demonstrated the worst performance, Revo Six showed better capabilities to produce a higher outlet temperature due to its longer liquefier section and cylindrically shaped heating block. Furthermore, the melt front for each hot end was studied for a full range of feed rates and extrusion set temperatures, and feed rate was found to be the dominating process parameter impacting the melt front location in each hot end.

1. The experimental procedure and computational modeling developed in this study can provide a template for systemic and comprehensive benchmarking of current and future hot-end assemblies. Furthermore, the results from this work can directly help 3D printer manufacturers enhance their printers' capabilities and optimize their printer design. The single-strand deposition model can be extended to incorporate multiple strands deposited adjacently, at varying layer heights and distances to explore the aforementioned effects on the strand cross-sectional areas. The effect of printing speed and feed rate can be further explored to characterize the impact of the velocity ratio (feed rate/printhead speed) on the cross-sectional geometries for various hot ends. Finally, a connection can be made between common 3D printer settings such as wall thickness, infill density and substrate temperature to assist in the slicing process when choosing a particular 3D printer and hot end assembly. In summary, the findings of this work can be defined as:
 - i. *Temperature versus Under-extrusion* Extrusion temperature significantly influences under-extrusion, impacting print quality.
 - ii. *Feed rate and Under-extrusion* Higher feed rates correlate with increased under-extrusion, affecting print consistency.
 - iii. *Hot end performance variation* Different hot end models exhibit varying levels of under-extrusion, emphasizing the importance of selecting the right model for optimal printing. Query ID="Q3" Text="Author contribution is mandatory for publication in this journal. Please provide the statement."

Acknowledgements This project was financed in part by a grant from the Commonwealth of Pennsylvania, Department of Community and Economic Development.

Author contributions M.H. and A.O. wrote the main manuscript and prepared the figures. B.E. and K.F. came up with concept, design of experiment and simulation. M.H. verified simulation with experimental procedure. All authors reviewed the manuscript.

Funding The authors have not disclosed any funding.

Data availability The authors declare that the data supporting the findings of this study are available within the paper. Should any raw data files be needed in another format they are available from the corresponding author upon reasonable request.

Declarations

Competing interests The authors have no financial or proprietary interests in any material discussed in this article.

Open Access This article is licensed under a Creative Commons Attribution 4.0 International License, which permits use, sharing, adaptation, distribution and reproduction in any medium or format, as long as you give appropriate credit to the original author(s) and the source, provide a link to the Creative Commons licence, and indicate if changes were made. The images or other third party material in this article are included in the article's Creative Commons licence, unless indicated otherwise in a credit line to the material. If material is not included in the article's Creative Commons licence and your intended use is not permitted by statutory regulation or exceeds the permitted use, you will need to obtain permission directly from the copyright holder. To view a copy of this licence, visit <http://creativecommons.org/licenses/by/4.0/>.

References

1. Turner BN, Strong R, Gold SA. A review of melt extrusion additive manufacturing processes: I. process design and modeling. *Rapid Prototyp J.* 2014;20(3):192–204. <https://doi.org/10.1108/RPJ-03-2013-0023>.
2. Jackson B, Fouladi K, Eslami B. Multi-parameter optimization of 3D printing condition for enhanced quality and strength. *Polymers.* 2022;14(8):1586. <https://doi.org/10.3390/polym14081586>.
3. Livolsi F, May T, Caputo D, Fouladi K, Eslami B. Multiscale study on effect of humidity on shape memory polymers used in three-dimensional printing. *J Manuf Sci Eng.* 2021;143(9):091010. <https://doi.org/10.1115/1.4049828>.
4. Lambos N, Vosniakos G-C, Papazetis G. Low-cost automatic identification of nozzle clogging in material extrusion 3D printers. *Proc Manuf.* 2020;51:274–9. <https://doi.org/10.1016/j.promfg.2020.09.030>.
5. Mackay ME, Swain ZR, Banbury CR, Phan DD, Edwards DA. The performance of the hot end in a plasticating 3D printer. *J Rheol.* 2017;61(2):229–36. <https://doi.org/10.1122/1.4974742>.
6. Xu X, Wanglin Q, Wan D, Wu J, Zhao F, Xiong Y. Numerical modelling of the viscoelastic polymer melt flow in material extrusion additive manufacturing. *Virtual Phys Prototyp.* 2024;19(1):e2300666. <https://doi.org/10.1080/17452759.2023.2300666>.
7. Pricci A, de Tullio MD, Percoco G. Semi-analytical models for non-Newtonian fluids in tapered and cylindrical ducts, applied to the extrusion-based additive manufacturing. *Mater Des.* 2022;223:111168. <https://doi.org/10.1016/j.matdes.2022.111168>.
8. Duty C, et al. What makes a material printable? A viscoelastic model for extrusion-based 3D printing of polymers. *J Manuf Process.* 2018;35:526–37. <https://doi.org/10.1016/j.jmapro.2018.09.024>.
9. CNC Kitchen (n.d.) Comparing PLA, PETG, & ASA [Feat. Prusament]. CNC Kitchen. <https://www.cnckitchen.com/blog/comparing-pla-petg-amp-asa-feat-prusament>. Retrieved 4 Sept 2024
10. Marlin (n.d.) What is Marlin? Marlin firmware. Retrieved from <https://marlinfw.org/docs/basics/introduction.html>. Retrieved 4 Sept 2024
11. Not Applicable (n.d.) Pronterface. Retrieved on 4 Sept 2024, from <https://www.pronterface.com/>
12. Optris PIX Connect Operator's Manual (n.d.) Optris GmbH. Retrieved from <https://www.instrumart.com/assets/PIX-Connect-Manual.pdf>. Retrieved on 4 Sept 2024
13. Wang J (2012) PVT properties of polymers for injection molding. In: Some critical issues for injection molding (pp 3–30). Retrieved from <https://core.ac.uk/download/478113163.pdf>
14. Manual U (2009) Ansys fluent 12.0.theory guide, p 67
15. Introducing Roto (n.d.) E3D-online. Retrieved from <https://e3d-online.com/blogs/news/introducing-roto>, Retrieved 4 Sept 2024
16. Geng P, et al. Effects of extrusion speed and printing speed on the 3D printing stability of extruded PEEK filament. *J Manuf Process.* 2019;37:266–73. <https://doi.org/10.1016/j.jmapro.2018.11.023>.
17. Mishra AA, Momin A, Strano M, Rane K. Implementation of viscosity and density models for improved numerical analysis of melt flow dynamics in the nozzle during extrusion-based additive manufacturing. *Progress Addit Manuf.* 2022. <https://doi.org/10.1007/s40964-021-00208-z>.
18. Serdeczny MP (2020) Numerical and experimental analysis of filament-based material extrusion additive manufacturing. Technical University of Denmark. Retrieved from <https://orbit.dtu.dk/en/publications/numerical-and-experimental-analysis-of-filament-based-material-ex>
19. Ufodike CO, Nzebuka GC. Investigation of thermal evolution and fluid flow in the hot-end of a material extrusion 3D Printer using melting model. *Addit Manuf.* 2022;49:102502. <https://doi.org/10.1016/j.addma.2021.102502>.
20. Gosset A, Barreiro-Villaverde D, Becerra Permyu JC, Lema M, Ares-Pernas A, Abad López MJ. Experimental and numerical investigation of the extrusion and deposition process of a poly (lactic acid) strand with fused deposition modeling. *Polymers.* 2020;12(12):2885. <https://doi.org/10.3390/polym12122885>.

21. Zhu HY, Xiao XT, Zhang ZH. Fitting and verification viscosity parameter of ABS/aluminum blends. *Adv Mater Res*. 2011;308–310:824–30.
22. Verma A, Vishnoi P, Sukhotskiy V, Furlani EP. Numerical simulation of extrusion additive manufacturing: fused deposition modeling. *TechConnect Briefs*. 2018;4:118–21.
23. Xie D, et al. Rheological, thermal, and degradation properties of PLA/PPG blends. *Materials*. 2019;12(21):3519. <https://doi.org/10.3390/ma12213519>.
24. Khoo RZ, Ismail H, Chow WS. Thermal and morphological properties of poly (lactic acid)/nanocellulose nanocomposites. *Proc Chem*. 2016;19:788–94. <https://doi.org/10.1016/j.proche.2016.03.086>.
25. Hutchinson MJ (2023) Benchmarking and investigation of 3D printer hot ends through combined numerical and experimental effort (Order No. 30488156). Available from Dissertations & Theses @ Widener University; ProQuest Dissertations & Theses A&I. (2811784965). Retrieved from <https://www.proquest.com/dissertations-theses/benchmarking-investigation-3d-printer-hot-ends/docview/2811784965/se-2>
26. Mendenhall R, Eslami B. Experimental investigation on effect of temperature on FDM 3D printing polymers: ABS, PETG, and PLA. *Appl Sci*. 2023;13(20):11503. <https://doi.org/10.3390/app132011503>.
27. Harding OJ, Griffiths CA, Rees A, Pletsas D. Methods to reduce energy and polymer consumption for fused filament fabrication 3D printing. *Polymers*. 2023;15:1874. <https://doi.org/10.3390/polym15081874>.

Publisher's Note Springer Nature remains neutral with regard to jurisdictional claims in published maps and institutional affiliations.